ventilation were different, were tested in a model house. The effects of the differences in the inlet conditions on the indoor thermal environment and human thermo-physiological responses were investigated by the coupled analysis of CFD and human thermal models. Finally, the maximum availability of natural ventilation was quantitatively discussed based on the result by a subjective experiment.

OUTLINE OF SIMULATIONS

CFD model

Figure 1 shows the target room in a model house located in Tokai city in Japan. The room size was 3.6 m (width; x direction) × 7.0 m (length; y direction) × 2.4 m (height; z direction). A 1.2 m (width) × 1.0 m (height) window was installed in the southern wall. A natural ventilation through the window and a 2.6 m (width) × 2.0 m (height) opening of the northern wall was considered in this study. The velocity and turbulence intensity of the incoming flow through the window were set at 1.0 m/s (constant) and 10 %, respectively. A human body model (rectangular box shape), whose size was 0.3 m (width) × 0.2 m (length) × 1.6 m (height), was arranged in the center of the room. In order to couple with the human thermal model described below, the human body model was divided into 32 segments, as shown in Figure 2. The CFD analysis conditions are summarized in Table 1.

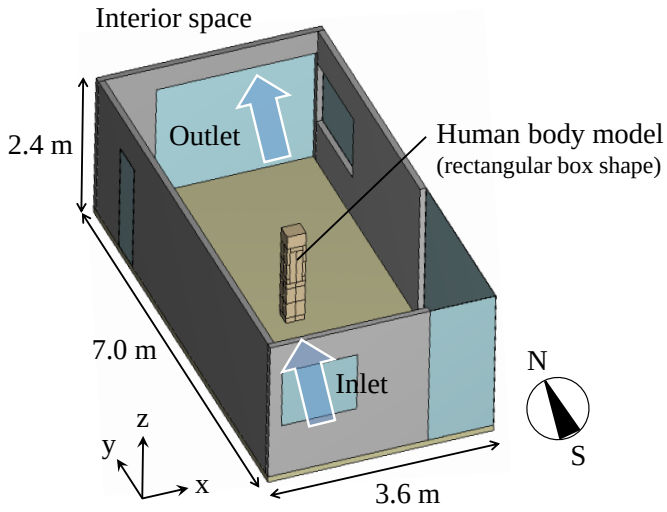

Figure 1. *Schematic view of the target room*

Human thermal model

A three-dimensional human thermal model proposed by Sakoi et al. (2006) was used in this study. Their model can predict local skin temperatures and local sensible and latent heat losses under non-uniform thermal environments and various clothing conditions. In this study, briefs, short-sleeve shirt, short pants, socks, and sports shoes were assumed as the clothing condition. The thermal resistance for the whole human body was set at 0.36 clo.

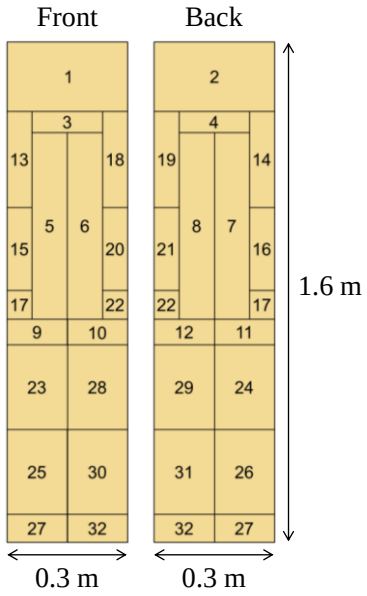

1	Face	2	Head
3	Neck (front)	4	Neck (back)
5	Chest (right)	6	Chest (left)
7	Back (right)	8	Back (left)
9	Waist (right-front)	10	Waist (left-front)
11	Waist (right-back)	12	Waist (left-back)
13	Right upper arm (front)	14	Right upper arm (back)
15	Right forearm (front)	16	Right forearm (back)
17	Right hand		
18	Left upper arm (front)	19	Left upper arm (back)
20	Left forearm (front)	21	Left forearm (back)
22	Left hand		
23	Right thigh (front)	24	Right thigh (back)
25	Right lower leg (front)	26	Right lower leg (back)
27	Right foot		
28	Left thigh (front)	29	Left thigh (back)
30	Left lower leg (front)	31	Left lower leg (back)
32	Left foot		

Figure 2. *32 segments of the human body model in CFD*

Table 1. *CFD analysis conditions*

1. Domain	3.6 m (x) × 7.0 m (y) × 2.4 m (z)
2. Grid points	45 (x) × 88 (y) × 33 (z) = 130,680
3. Scheme for convection terms	QUICK scheme for all governing equations
4. Turbulence model	RNG k-ε model (high-Reynolds number type)
5. Inlet boundary conditions	Velocity : 1.0 m/s (10 % turbulence intensity) Temperature : 28-35 °C (cf. Table 2) Humidity : 50 % RH
6. Outlet boundary conditions	Zero-gradient conditions for all variables
7. Solid boundary conditions	Velocity : Logarithmic law Temperature : Overall heat transfer coefficients for the outer walls, inner walls, ceiling, floor, and window were 0.5, 0.3, 0.35, 0.3, and 2.08 W/(m^2·K), respectively. Humidity : Impermeable condition without condensation
8. Heat generation (from human body)	Sensible heat : Results from the human thermal model Latent heat : 63 W (constant)

Coupling method of CFD and human thermal models

The CFD and human thermal models described above were coupled every 10 minutes. Using the convective and radiative heat transfer coefficients, indoor mean temperature and humidity, and mean wall surface temperature (for all walls) calculated by the CFD results, the human thermal model predicted local skin temperatures and local heat losses (convective, radiative, and evaporative heat losses). Then, using the convective and radiative heat losses from the human body predicted by the human

thermal model as the CFD boundary conditions, CFD analysis was performed. With regard to evaporative heat loss from the human body, a constant value (63 W) from the head was given in the CFD analysis. In the human thermal model, on the other hand, evaporative heat loss from the human body varied locally and temporally. In the next phase of this study, a coupling method of all (convective, radiative, and evaporative) heat losses will be introduced.

SIMULATED CASES

Table 2 shows the simulated cases. A total of 24 cases were conducted. The differences among the simulated cases were the angle and temperature of the incoming flow for natural ventilation. Here, the combinations of three angles (0°, 20°, and 40°) and eight temperatures (28-35 °C) were tested as the inlet conditions.

Table 2. *Simulated cases*

	Inlet condition			Inlet condition	
	Inflow angle	Temperature		Inflow angle	Temperature
Case 1-1	0°	28 °C	Case 5-1	0°	32 °C
Case 1-2	20°		Case 5-2	20°	
Case 1-3	40°		Case 5-3	40°	
Case 2-1	0°	29 °C	Case 6-1	0°	33 °C
Case 2-2	20°		Case 6-2	20°	
Case 2-3	40°		Case 6-3	40°	
Case 3-1	0°	30 °C	Case 7-1	0°	34 °C
Case 3-2	20°		Case 7-2	20°	
Case 3-3	40°		Case 7-3	40°	
Case 4-1	0°	31 °C	Case 8-1	0°	35 °C
Case 4-2	20°		Case 8-2	20°	
Case 4-3	40°		Case 8-3	40°	

RESULTS AND DISCUSSION

Indoor thermal and airflow environments

As an example, Figure 3 shows the horizontal distributions of the air temperature and velocity vectors at a height of 1.2 m in Cases 5-1 to 5-3 (Inflow temperature: 32 °C). Although the air temperatures are different from those in other cases due to the difference in the inflow temperature (cf. Table 2), the airflow patterns are almost the same among the cases with the same inflow angle (e.g., Case 5-1 and Case 1-1).

In Case 5-1 (0° inflow angle; Figure 3(1)), the incoming flow straightly goes through the right-hand side region of the human body model, while it flows through the left-hand side region of the human body in Case 5-3 (40° inflow angle; Figure 3(3)). Although the flow patterns are different, the airflow around the human body is relatively calm in both cases. In Case 5-2 (20° inflow angle; Figure 3(2)), on the other hand, the incoming flow blows against the human body and a complex airflow is formed around the human body.

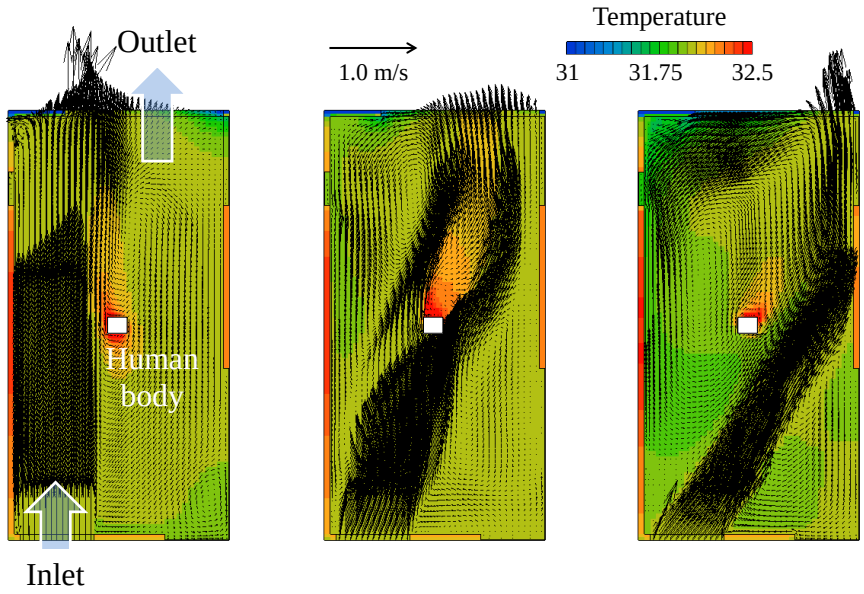

(1) Case 5-1 *(2) Case 5-2* *(3) Case 5-3*

Figure 3. *Horizontal distributions of the air temperature and velocity vectors at a height of 1.2 m*

Effects of the inflow angle for natural ventilation

Figure 4 shows the local skin temperatures and local heat losses (convective, radiative, and evaporative heat losses) predicted by the human thermal model in Cases 5-1 to 5-3 (Inflow temperature: 32 °C).

In Case 5-1 (0° inflow angle; Figure 4(1)), the local skin temperatures have a range of 34.1-35.1 °C. In the face, head, neck, chest, back, and waist (Segment No. 1-12), the evaporative heat loss is larger than the convective and radiative heat losses, while there is little difference among the three heat losses in other segments. In the human thermal model conducted in this study, the local sweating is defined based on the local sweating response under a threshold limit; therefore, the segments such as head, chest, and back may be easy to get sweaty. Further investigation on this matter will be conducted in the next phase of this study.

In Case 5-2 (20° inflow angle; Figure 4(2)), the local skin temperatures have a range of 33.7-34.7 °C and are generally lower than those in Case 5-1. The convective heat loss in Case 5-2 is about two to five times larger than that in Case 5-1 because the incoming flow blows against the human body (cf. Figure 3(2)), and, as a result, the skin temperatures become lower in Case 5-2. Furthermore, the lower skin temperatures cause the smaller radiative heat loss and also the smaller sweating and evaporative heat loss.

In Case 5-3 (40° inflow angle; Figure 4(3)), the local skin temperatures and local heat losses are almost the same as those in Case 5-1. This is mainly because relatively calm airflow environments are formed around the human body in both cases (cf. Figures 3(1) and (3)), as described in the previous section.

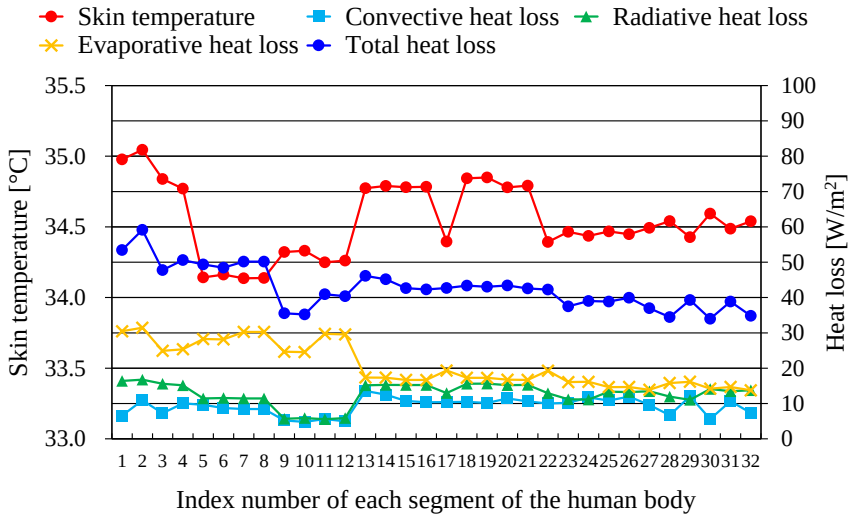

(1) Case 5-1

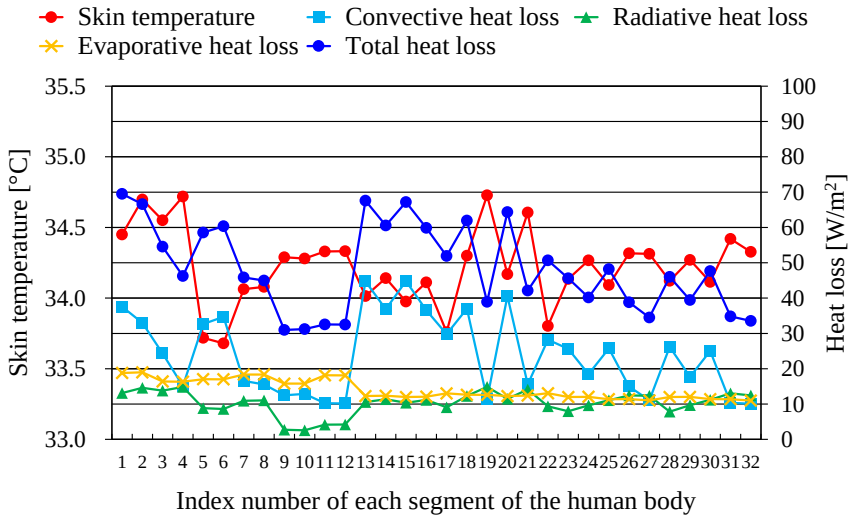

(2) Case 5-2

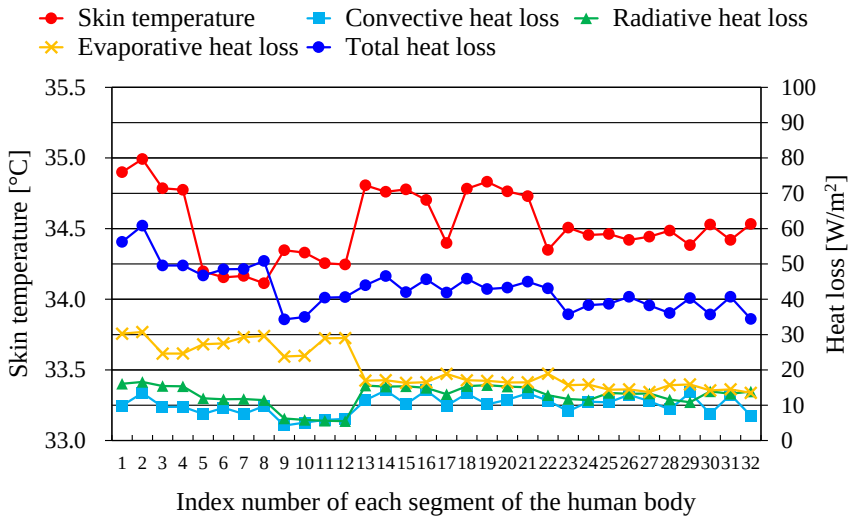

(3) Case 5-3

Figure 4. *Skin temperature and heat loss in each segment of the human body*

Effects of the inflow temperature for natural ventilation

Figure 5 shows the sums of each heat loss in all segments of the human body and the mean skin temperature averaged over four local skin temperatures in the chest (left), left forearm (front), left thigh (front), and left lower leg (front). In both the cases with 0° inflow angle (Figure 5(1)) and 20° inflow angle (Figure 5(2)), as the inflow temperature increases, the mean skin temperature and the evaporative heat loss become higher/larger, while the convective and radiative heat losses as well as the total heat loss are smaller.

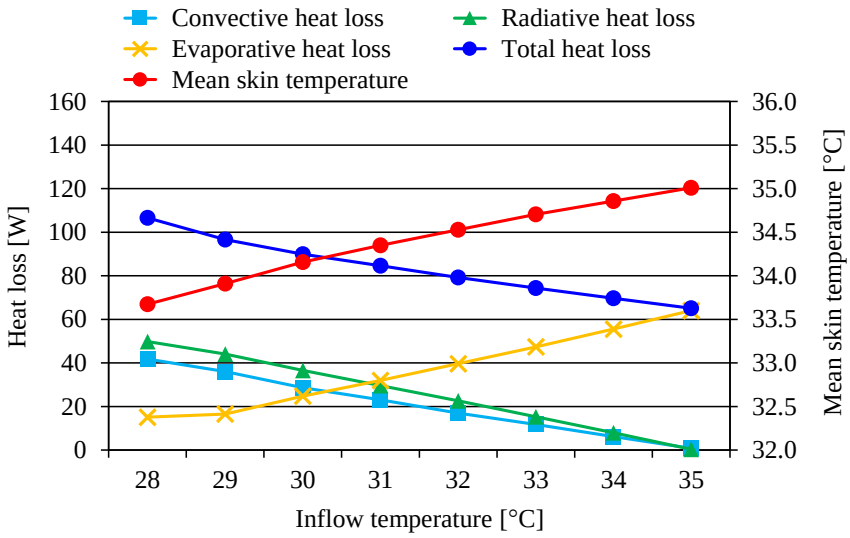

(1) Cases with 0° inflow angle

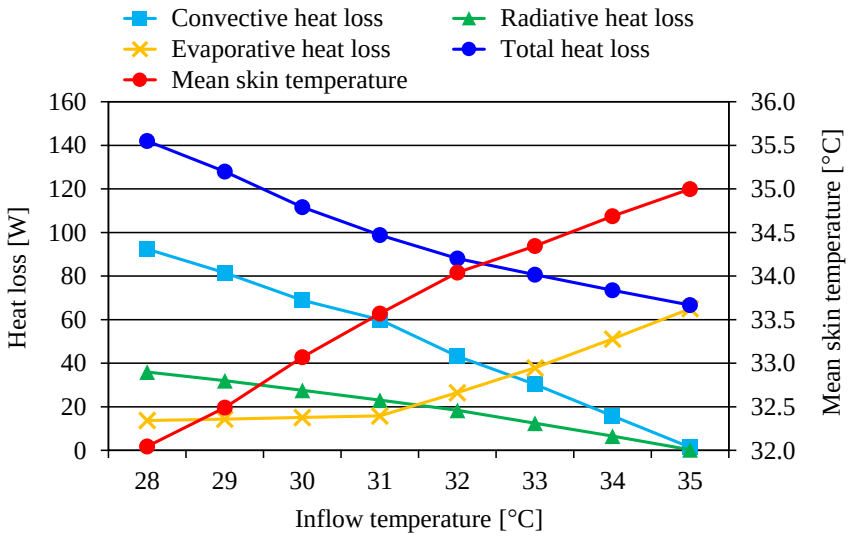

(2) Cases with 20° inflow angle

Figure 5. *Changes of heat losses and mean surface temperature with the inflow temperature*

According to a subjective experiment under natural ventilation in a model house conducted by Ota (2014), the mean skin temperature without discomfort is 34.5 °C or less. Judging from the result, when the airflow around the human body is relatively calm (in the cases with 0° (or 40°) inflow angle), the inflow temperature is allowed up to 32 °C. On the other hand, when the incoming flow blows against the human body (in the cases with 20° inflow angle), the allowance of the inflow temperature expands up to 33.5 °C.

CONCLUSIONS

In this study, a coupled analysis of CFD and human thermal models on the indoor thermal environment and human thermophysiological responses under natural ventilation in a model house was performed. In particular, the effects of the differences in the inlet conditions (the angle and temperature of the incoming flow for natural ventilation) on the indoor thermal environment and human thermo-physiological responses were investigated. Finally, the maximum availability of natural ventilation was quantitatively discussed based on the result by a subjective experiment.

ACKNOWLEDGEMENTS

This study was supported by a Grant-in-Aid for Scientific Research (A) No. 24246098 from the Japan Society for the Promotion of Science (JSPS). The authors would like to express their gratitude to Mr. S. Shiba (Takenaka Corporation, Japan) and Dr. Y. Xuan (Nagoya University) for their valuable contributions to this study.

REFERENCES

Sakoi, T., Tsuzuki, K., Kato, S., Ooka, R., Song, D., and Zhu, S. 2006. A three-dimensional human thermal model for non-uniform thermal environments, *Thermal Manikins and Modelling: Proceedings of the 6th International Thermal Manikin and Modelling Meeting*, pp.77-88.

Ota, S. 2014. A study on thermal comfort caused by natural ventilation and sunshine in the indoor environment of housing, *Master's Thesis*, Nagoya University (Japan).